



GasHis-Transformer: A Multi-scale Visual Transformer Approach for Gastric Histopathological Image Classification

Haoyuan Chen^a, Chen Li^{a,*}, Ge Wang^{b,*}, Xiaoyan Li^c, Weiming Hu^a, Yixin Li^a, Wanli Liu^a, Changhao Sun^{a,d,e}, Marcin Grzegorzec^c

^aMicroscopic Image and Medical Image Analysis Group, College of Medicine and Biological Information Engineering, Northeastern University, 110169, Shenyang, PR China

^bDepartment of Biomedical Engineering, Rensselaer Polytechnic Institute, 12180, Troy, New York, USA

^cDepartment of Pathology, Cancer Hospital, China Medical University, Liaoning Cancer Hospital and Institute, 110042, Shenyang, PR China

^dUniversity of Chinese Academy of Sciences, 100049, Beijing, PR China

^eInstitute of Medical Informatics, University of Lübeck, 23538, Lübeck, Germany

ARTICLE INFO

Article history:

Gastric histopathological image, Multi-scale visual transformer, Image classification

ABSTRACT

Existing deep learning methods for diagnosis of gastric cancer commonly use convolutional neural network. Recently, the *Visual Transformer* has attracted great attention because of its performance and efficiency, but its applications are mostly in the field of computer vision. In this paper, a multi-scale visual transformer model, referred to as GasHis-Transformer, is proposed for *Gastric Histopathological Image Classification* (GHIC), which enables the automatic classification of microscopic gastric images into abnormal and normal cases. The GasHis-Transformer model consists of two key modules: A global information module and a local information module to extract histopathological features effectively. In our experiments, a public hematoxylin and eosin (H&E) stained gastric histopathological dataset with 280 abnormal and normal images are divided into training, validation and test sets by a ratio of 1 : 1 : 2. The GasHis-Transformer model is applied to estimate precision, recall, F1-score and accuracy on the test set of gastric histopathological dataset as 98.0%, 100.0%, 96.0% and 98.0%, respectively. Furthermore, a critical study is conducted to evaluate the robustness of GasHis-Transformer, where ten different noises including four adversarial attack and six conventional image noises are added. In addition, a clinically meaningful study is executed to test the gastrointestinal cancer identification performance of GasHis-Transformer with 620 abnormal images and achieves 96.8% accuracy. Finally, a comparative study is performed to test the generalizability with both H&E and immunohistochemical stained images on a lymphoma image dataset of 374 images and a breast cancer dataset of 1390 images, producing comparable F1-scores (85.6% and 82.8%) and accuracies (83.9% and 89.4%), respectively. In conclusion, GasHis-Transformer demonstrates high classification performance and shows its significant potential in the GHIC task.

© 2021 Elsevier B. V. All rights reserved.

*Corresponding author:

e-mail: lichen201096@hotmail.com (Chen Li), wangg6@rpi.edu (Ge Wang)

1. Introduction

Cancer is a malignant tumor that originates from epithelial tissue and it is one of the deadliest diseases Yis *et al.* (2019), which caused approximately 9.6 million deaths in 2018—the highest number since records began in the 1970s Chan *et al.* (2001). Of all cancer categories, gastric cancer has the second highest cancer rate in the world in terms of morbidity and mortality Chan *et al.* (2001). Gastric cancer is a collection of abnormal cells that form tumors in the stomach. In histopathology, the most common type of gastric cancer is adenocarcinoma, which starts in mucous-producing cells in the inner layer of the stomach that tend to invade the stomach wall, infiltrating the muscular mucosa and then invade the outer muscular. About 800,000 people die of the disease every year, according to World Health Organization statistics Sharma *et al.* (2015). In countries around the world, the number of gastric cancer patients is rising faster than the number of non-cancer patients. It is estimated that about 30,000 new cases of gastric cancer occur each year Korkmaz *et al.* (2017). Therefore, it is essential for medical staffs to accurately diagnose gastric cancer.

The diagnosis of gastric cancer depends on a careful examination of Hematoxylin and Eosin (H&E) stained sections by pathologists under a microscope. It is time-consuming and subjective to observe tissue slices under a microscope Elsheikh *et al.* (2013). Because of these shortcomings, pathologists have a great deal of difficulties with accurate screening and diagnosis of gastric cancer. Thus, computer-aided diagnosis (CAD) that began in the 1980s can reduce these shortcomings by making diagnostic decisions and improving efficiency Doi (2007). The goal of CAD is to improve the diagnosis quality and efficiency of medical doctors by image processing, pattern recognition, machine learning and machine vision methods Doi (2005). Over the past few decades, researchers have conducted extensive research on the design of CAD that assists doctors to diagnose cancer and treat the disease.

With the advent of the era of artificial intelligence, deep learning becomes the most extensive and widely used method of CAD Asiri *et al.* (2019). Deep learning works in many research

fields, such as data mining, machine learning, natural language processing, multimedia learning, computer vision, recommendation algorithms and personalization technology. It enables a computer to imitate human activities, solves many complex pattern recognition problems and makes great progress in artificial intelligence-related techniques LeCun *et al.* (2015). In the field of artificial intelligence, *Convolutional Neural Network* (CNN) models are the dominant type of deep learning that can be applied to many machine vision tasks LeCun *et al.* (1989). However, there are some shortcomings of CNN models, one of which is that CNN models do not handle global information well. In contrast, the novel *Visual Transformer* (VT) models applied in the field of computer vision can support more abundant global information. Based on CNN and VT models mentioned above, a hybrid model is heuristically proposed for *Gastric Histopathological Image Classification* (GHIC) tasks, namely GasHis-Transformer, to integrate the local and global information into an organic whole. The architecture of GasHis-Transformer is shown in Fig. 1.

The proposed GasHis-Transformer model can be understood as an early fusion of a transformer model and a CNN model. The whole model is made up of two modules, namely Global Information Module (GIM) and Local Information Module (LIM). First, based on BoTNet-50 Srinivas *et al.* (2021), we design GIM to extract abundant global information to describe a gastric histopathological image as a whole. Then, we follow the parallel structure idea of Inception-V3 Szegedy *et al.* (2016) to obtain multi-scale local information to represent the details of a gastric histopathological image.

The contributions of this paper are as follows:

- First, considering the advantages of VT and CNN models, our GasHis-Transformer model is proposed, which integrates the describing capability of global information and local information of VT and CNN.
- Second, in GasHis-Transformer, the idea of multi-scale image analysis is introduced to describe the details of gastric tissues and cells under a microscope.

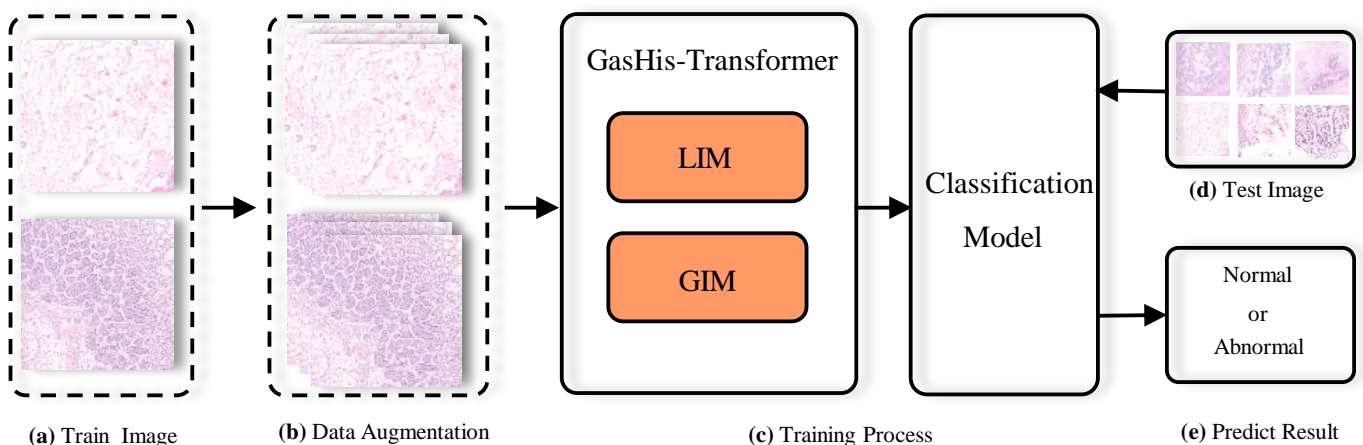


Fig. 1: The GasHis-Transformer model architecture.

- Third, GasHis-Transformer not only obtains good classification performance on gastric histopathological image dataset, but also shows an excellent generalization ability on other histopathological image datasets.

This paper is organized with five sections: Section 2 provides a review of the current status of GHIC tasks in the past few years, Section 3 introduces the details of the proposed GasHis-Transformer model, Section 4 presents experimental results. Finally, Section 5 closes the whole work with a brief conclusion.

2. Related Work

2.1. Image Classification in Gastric Histopathological Research

In GHIC tasks, traditional machine learning is an effective method that has been used for many years Yassin *et al.* (2018). In Sharma *et al.* (2015), 31 features based on color, texture and morphology extracted from each image patch are classified by an AdaBoost classifier and the final image classification result is obtained by combining the classification results of each patch. In Sharma *et al.* (2017), Random Forest (RF) classifier is used to classify 332 global graph features including the mean, variance, skewness, kurtosis and other features extracted from gastric cancer histopathological images. In Korkmaz and Binol (2018), after feature dimensionality reduction, Local Binary Patterns (LBP) and Histograms of Oriented Gradient (HOG) features are classified and compared by RF and Artificial Neural Network (ANN) classifiers. In Liu *et al.* (2018), three comparative experiments are carried out. K-Singular Value Decomposition (K-SVD) is first used to learn the features extracted from a CNN, and then sparse decomposition is carried out. Finally, a 95% classification accuracy is obtained.

In recent years, deep learning methods have become increasingly used in GHIC tasks. In Garcia *et al.* (2017), the improved ResNet-v2 network is used to classify images by adding an average pooling layer and a convolution layer. Finally, the classification accuracy of the model is 86.5%. In Song *et al.* (2020), 2166 whole slide images (WSIs) are classified by a deep learning model based on DeepLab-V3 with ResNet-50 architecture as the backbone and the accuracy, sensitivity and specificity of the model are 87.3%, 99.6% and 84.3%, respectively. In Kosaraju *et al.* (2020), a multi-scale receptive field deep neural network based on Inception-V3 model is proposed to analyze the histopathological images in WSIs. In Cho *et al.* (2020), a network is proposed to combine AlexNet, ResNet-50 and Inception-V3, then it uses ten-fold validation to test the classification performance. Finally, all the ten-fold validation results are used to calculate the accuracy, sensitivity and specificity.

2.2. Overview of Deep Learning Methods

The first application of deep learning model is LeNet proposed by LeCun *et al.* in 1989 LeCun *et al.* (1989). However, due to poor computing power, limited relative technology and negligible available data for analysis, deep learning does not exhibit excellent recognition performance in image classification. In 2012, Hinton *et al.* proposed AlexNet and used

compute unified device architecture to accelerate the training of deep learning models for the first time. AlexNet uses the powerful parallel computing ability of the graphics processing unit to process a large number of matrix operations in the training of deep learning model Krizhevsky *et al.* (2012). Since then, deep learning methods have formally replaced traditional machine learning methods. VGG model was proposed by the Visual Geometry Group at the University of Oxford in 2014. Its novelty contribution is raising the depths of networks from eight to sixteen or nineteen which is named VGG-16 and VGG-19, and turning large convolution kernels such as 7×7 and 5×5 into three or two 3×3 small convolution kernels Simonyan and Zisserman (2014). It is one of the milestones in deep learning after AlexNet and also the baseline for comparing new methods in deep learning field. VGG model has substantial advantages. First, VGG model uses the small convolution kernel to reduce parameters and improve the recognition accuracy. Second, VGG structure is consistent and suitable for parallel acceleration. Finally, the particularly important contribution is providing a clear direction for deep learning networks: increasing network depth Rawat and Wang (2017). However, VGG model also has some celebrated disadvantages. VGG model only increases the number of network layers as well as large parameters, resulting in long training time. In addition, when VGG model reaches certain depth, the gradient simply disappears, which makes the model difficult to optimize.

Inception-V3 model is the other method to modify AlexNet and based on the GoogLeNet proposed by Szegedy *et al.* in 2015 Szegedy *et al.* (2015). Instead of using the conventional method to increase the number of network layers, Inception-V3 uses a novel convolution method to decompose the large filter sizes: using parallel convolution and factorized convolution in the same receptive fields, and the whole decomposition module is called the inception structure. Inception-V3 network has five different inception structures, each with its own set of components. The five inception modules are shown in Fig. 2. Inception-V3 model has obvious merits. Inception-V3 model uses inception module instead of large convolution kernel and global average pooling layer instead of full connection layer (FC layer) to prominently reduce the number of parameters compared with other networks which increased network layers so that it has an excellent performance on large-scale data sets and mobile devices with poor computing ability Rawat and Wang (2017). However, the fatal drawback of Inception-V3 model is that training is very difficult and even cannot lead to convergence when the network depth is increasing.

ResNet model proposed by He *et al.* in 2015 perfectly solves the shortcomings of VGG and Inception-V3 by increasing the number of network layers leading to the disappearance of gradients and the non-convergence of the model. ResNet models are named as ResNet-18, ResNet-32, ResNet-50, ResNet-101 and ResNet-152 according to the number of 18, 32, 50, 101 and 152 network layers He *et al.* (2016). The main contribution of ResNet model is to propose residual structure and apply residual structure to deep learning networks for the first time. There are two main design ideas for residuals: shortcut connection and identity mapping. Shortcut connection makes residuals

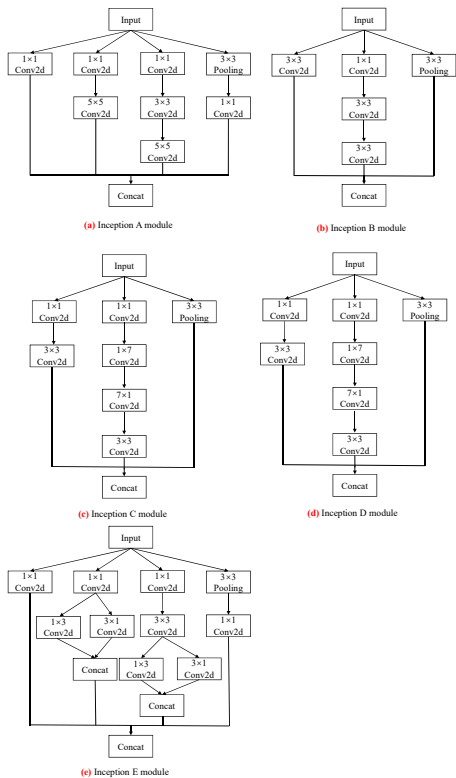


Fig. 2: Five modules of Inception-V3 model.

possible and identity mapping makes the network deeper. The residual learning unit of ResNet model is used to connect results of multiple convolution layers with an identity mapping using a shortcut connection by ReLU activation function. There are two types of residual unit structures, namely, two-layer residual unit and three-layer residual unit. Two-layer residual units are used in shallower network layers, such as ResNet-18 and ResNet-32; three-layer residual units are used in models with deeper network layers, such as ResNet-50 and ResNet-101 He et al. (2016). ResNet model, as the first network to present the widely used residual structure, has many remarkable advantages. First of all, it has epoch-making significance that ResNet model introduces residual structure to solve the model degeneration problem caused by the deepening network layer. Secondly, Resnet model uses normalized initialization and intermediate normalized layer to better solve the problem of gradient disappearance. However, ResNet model has some common shortcomings of CNN models. First, the parameters used to increase the pooling layer of the receptive field cannot be trained. In addition, the model has poor ability to extract features from small objects Lu et al. (2020).

Inspired by deep separable convolution Sifre and Mallat (2014), Xception is an improvement of Inception-V3 proposed by Google Szegedy et al. (2016); Chollet (2017). Xception divides depthwise separable convolution into depthwise convolution and pointwise convolution to improve Inception structure. Concomitantly, residual connection He et al. (2016) is used in each block instead of concat in the original Inception structure. The advantage of Xception is that it combines the residual

structure and inception structure to integrate their advantages, and depthwise separable convolution reduces the complexity of the network, which makes the network model easy to convergence Howard et al. (2017). However, Xception also inherits the shortcomings of CNN models, in that the model has poor ability to extract global features.

In recent years, attention mechanisms have good performance in image classification tasks, such as Non-local+Resnet Wang et al. (2018), CBAM+Resnet Woo et al. (2018), SENet+CNN Hu et al. (2018), GCNet+Resnet Cao et al. (2019), HCRF-AM Li et al. (2021) and VT models Vaswani et al. (2017). VT models are more and more used in image classification, image segmentation, object detection and other computer vision fields Han et al. (2020). There are two main forms of VT model in image classification task, that is the pure self-attention structure represented by Vision Transformer(ViT) Khan et al. (2021) and the self-attention structure combined CNN models represented by BoTNet-50 Srinivas et al. (2021); Khan et al. (2021); Dosovitskiy et al. (2020). The biggest advantage of transformer models is that they perfectly solve the shortcomings of CNN models. VT models can better describe the global information of images and have a good ability to extract global information by introducing an attention mechanism. Meanwhile, VT models have some disadvantages. The excellent performance of the transformer model in natural language processing depends on the data scale of at least one million. However, most datasets applied in the field of computer vision are in thousands level. Therefore, the effect of ViT in dealing with small or medium-sized datasets, such as Imagenet, is not even as good as ResNet model, and it performs well only on large-scale datasets Dosovitskiy et al. (2020).

3. GasHis-Transformer

3.1. Vision Transformer (ViT)

The first model for training large-scale datasets using Transformer instead of standard convolution in computer vision field is ViT Khan et al. (2021); Dosovitskiy et al. (2020). An overview of ViT model is shown in Fig. 3(a). To handle a 2D image as a 1D sequence, 2D patch sequence $x_p \in \mathbb{R}^{N \times (P^2 \times C)}$ is obtained by reshaping the original image $x \in \mathbb{R}^{H \times W \times C}$. C is the number of image's channels, $(H \times W)$ is the size of each original iamge, (P^2) is the size of each image patch, $N = HW/P^2$ is the sum of patch number as the same as input sequence length of the transformer encoder. Because the invariant hidden vector size D which is used in the transformer goes through all layers, where all patches are flattened to D dimensions, and D dimensions (patch embeddings) are mapped by a linear projection which can be trained. To retain positional information, the sequence of embedding vectors combines standard 1D position embedding and patch embeddings are selected to be the input of the transformer encoder.

Transformer encoder is composed of multiple alternate *Multi Head Self-Attention* (MHSA) blocks Srinivas et al. (2021) and multilayer perceptron (MLP) blocks Vaswani et al. (2017). A structure of transformer encoder is shown in Fig. 3(b). Layer-norm (LN) is used in front of each layer and connected to the

following block through residual connection. MLP block has two network layers, which is connected by a non-linear gaussian error linear units (GELU) activation function. Finally, for

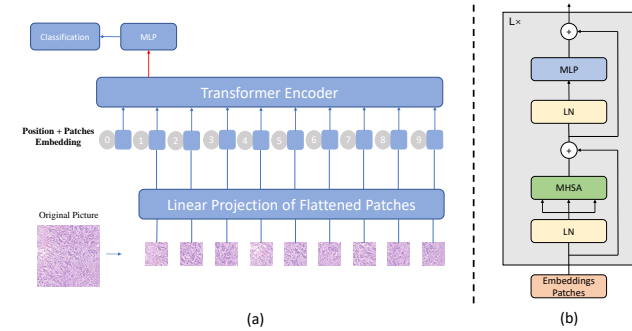


Fig. 3: The details of ViT model. (a) is an overview of ViT model training process. (b) is a structure of transformer encoder.

classification, a MLP block with a hidden layer is used to train the features which are trained by transformer encoder. In the fine-tuning process, only a single linear layer is used.

3.2. BoTNet

BoTNet-50 Srinivas et al. (2021) is a VT model which combines ResNet-50 with the MHSA layer. Because the usage of the MHSA layers reduces massive parameters, BoTNet-50 is a network with a simple structure and powerful functions. A architecture of BoTNet-50 model is compared to ResNet-50 are shown in Fig. 4. BoTNet-50 is not used sophisticated and luxuriant structure, only makes some basic modifications on ResNet-50. Similarly to the hybrid model of ViT Dosovitskiy et al. (2020), in which input sequence extracted from CNN models to alter raw image patches, BoTNet-50 remains the model of ResNet-50 in advance of stage c4 and using the

MHSA layers substitute for the last three 3×3 spatial convolutions in stage c5 of the model of ResNet. Thus, BoTNet-50 obtains the global self concern in 2D feature maps. The latter part is the same as ResNet-50. The average pooling layer and FC layer are used to extract features and obtain classification results.

There are some different places between BoTNet-50 and ViT. The main difference is that the MHSA Vaswani et al. (2017) of ViT uses standard 2D sequence position encoding, while BoTNet-50 uses 2D relative position encoding. The latest results Bello et al. (2019); Shaw et al. (2018); Ramachandran et al. (2019) show that relative position encoding is more suitable for image classification tasks than traditional encoding. A structure of relative position encoding of the MHSA is shown in Fig. 5. There are four sets of single-headed attention in each MHSA layer of BoTNet-50. At present, the structure of Fig. 5 only takes one single-headed attention as example. First, for a given pixel $x_{ij} \in \mathbb{R}$, we extract $ab \in N_k(i, j)$ from the spatial extent k which centered on x_{ij} . Second, W_Q, W_K and W_V are defined as the learnable transforms and can compute the queries $q_{ij} = W_Q x_{ij}$, keys $k_{ab} = W_K x_{ab}$ and values $v_{ab} = W_V x_{ab}$, which are linear transformations of the pixels of spatial extent. The content information multiply the queries and keys value vectors. Thirdly, R_h and R_w are defined as the separable relative position encodings of height and weight are expressed by row offset $(a - i)$ and column offset $(b - j)$. The row offset and column offset are shown in Fig. 6 and they are connected with an embedding r_{a-i} and r_{b-j} . The row offset and column offset embeddings (position information) are connected to form $r_{a-i, b-j}$. Finally, the content information and position information are accumulated, and then the spatial-relative attention y_{ij} of the pixel x_{ij} is obtained by multiplying the aggregation results with

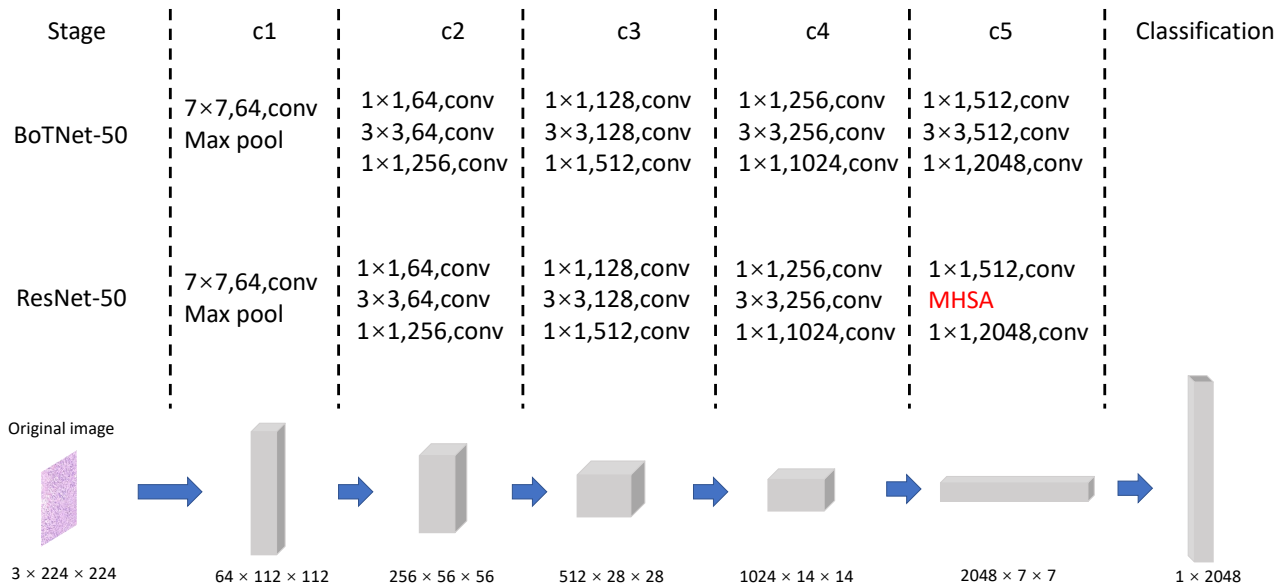


Fig. 4: The architecture of BoTNet-50 and ResNet-50.

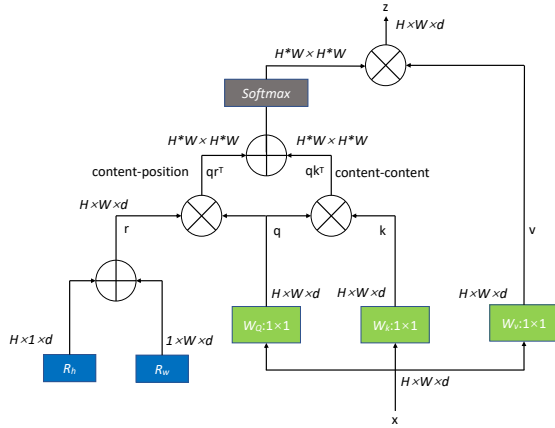


Fig. 5: The structure of relative position encoding of the MHSA. \oplus and \otimes express sum and matrix multiply respectively.

-1, -1	-1, 0	-1, 1	-1, 2
0, -1	0, 0	0, 1	0, 2
1, -1	1, 0	1, 1	1, 2

Fig. 6: A single example of relative distance computation. The relative distance in the figure is calculated according to the bright position. Red is row offset and blue is column offset.

values through softmax Shaw et al. (2018) as shown in Eq. 1.

$$y_{ij} = \sum_{a,b \in N_k(i,j)} \text{softmax}(q_{ij}^T k_{ab} + q_{ij}^T r_{a-i,b-j}) v_{ab} \quad (1)$$

The number of parameters in MHSA layer is different from that in convolution layer. The number of parameters in convolution increases at a quadratic rate with the increase of spatial extent, while the MHSA layer does not change with the change of spatial extent. When the sizes of input and output are the same, the computational cost of MHSA layer is far less than that of convolution in the same spatial extent. For example, when the input and output are 128-dimensionalities, the computational cost of 3 spatial extents in the convolution layer is the same as that of 19 spatial extents in the MHSA layer Shaw et al. (2018). Therefore, the parameters and computation time of BoTNet-50 are less than that of ResNet-50 Srinivas et al. (2021).

3.3. GasHis-Transformer

GasHis-Transformer model is proposed to classify gastric cancer histopathological image and its structure is shown in Fig. 7. GasHis-Transformer applies image normalization to improve the image quality Finlayson et al. (1998). This operation remains the image global information, only modifies the pixels to a specified range to accelerate the convergence of training model.

In Fig. 7 (a), normal and abnormal gastric hispathological images are used as training data for GasHis-Transformer.

In Fig. 7 (b), the shallow color of gastric cancer histopathological images and the implicit boundary characteristics of the nucleus results in poor image quality. This operation remains the image global information, only modifies the pixels to a specified range to accelerate the convergence of training models. The specific role of normalization is to summarize the statistical distribution of unified samples through the statistical probability of samples in events to train or predict deep learning models. When the input image pixels of all samples are positive, the weights connected with the first hidden layer neurons can only increase or decrease at the same time, resulting in a slow learning speed. To avoid this situation and speed up the model learning process, the input image pixels are normalized, which can reduce the mean and variance of the input pixels of all samples Finlayson et al. (1998). Furthermore, because of the multi-scale characteristics of histopathological images under the microscope, GasHis-Transformer augments the images by rotating and mirroring operations.

In Fig. 7 (c), images are used to train the proposed model, and this step is the core of the whole structure. GasHis-Transformer includes two parts: Global Information Module (GIM) and Local Information Module (LIM). In GIM, GasHis-Transformer follows the idea of BoTNet-50 which convolution layer in the last residual layer of the ResNet-50 model is replaced by the MHSA Srinivas et al. (2021). GIM retains all the structures before c5 stage of BoTNet-50 and 2048-dimensional global features are extracted in the last pooling layer of GIM. In LIM, GasHis-Transformer follows the idea of Inception-V3 and carries out a series of modifications to the traditional model. To match the standard input of GIM and make the features extracted by GIM and LIM in the whole network with the same measurement, LIM modifies the standard input size of Inception-V3 Szegedy et al. (2016) model from 299×299 to 224×224 and modifies the standard output size of every convolution layer and pooling layer in GasHis-Transformer. Similar to GIM, 2048-dimensional local features are extracted in the last pooling layer of LIM. At the end of GIM and LIM, the global and local features are fused to obtain the 4096-dimensional splicing feature as the final feature trained. Because many extracted features can increase the probability of extracting noise leading to overfitting Huang et al. (2019), GasHis-Transformer adds a dropout layer after concatenating features and filter out irrelevant features such as noise by discarding neurons with a certain probability Srivastava et al. (2014); Baldi and Sadowski (2013). Since the number of features extracted from each model in series with GIM and LIM is doubled, GasHis-Transformer set the probability to 0.5 and randomly discard half of them. Finally, GasHis-Transformer takes the output from the dropout layer as the input FC layer, and output it through the softmax Liu et al. (2016) function. The highest probability result is the classification of the results of gastric cancer. The whole proceeding of the proposed GasHis-Transformer network is shown in Algorithm 1.

In Fig. 7 (d), testing images including normal and abnormal are used to evaluate the classification performance of GasHis-Transformer.

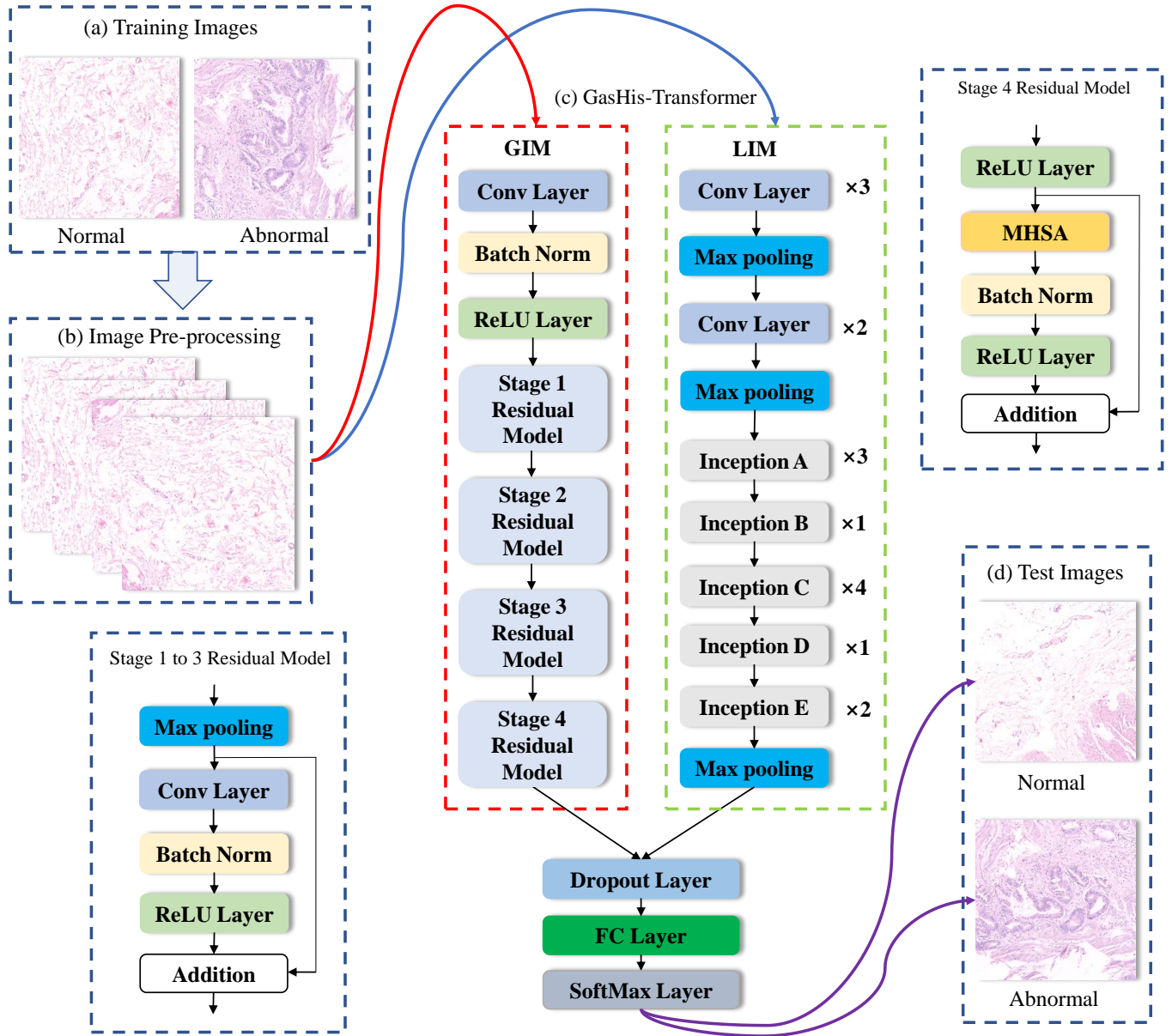


Fig. 7: The structure of GasHis-Transformer model.

4. Experiment Result and Analysis

4.1. Experimental Setting

4.1.1. Dataset

In this paper, an open source Haematoxylin and Eosin (H&E) stained gastric histopathological image dataset (HE-GHI-DS) is used in the experiment to evaluate the classification performance of GasHis-Transformer Sun et al. (2020). Hematoxylin stained solution is alkaline, which makes chromatin in the nucleus and ribosome in cytoplasm purple-blue; Eosin stained solution is acidic, which makes the components in cytoplasm and extracellular matrix red Miettinen et al. (2003). The images are part of the whole slide images (WSIs) in '*.tiff' format, where they are magnified 20 times and the image size is 2048×2048 pixels Li et al. (2018). HE-GHI-DS includes 140 normal im-

ages and 560 abnormal images. In the normal images, the nuclei are stable and arrange regularly and the nucleo-cytoplasmic ratio is small Burkhardt (2012). On contrary, in the abnormal images, the nucleus is abnormally large and irregular in features of dish or crater. Some examples of normal and abnormal gastric histopathological images are shown in Fig. 8.

4.1.2. Data Settings

Due to the imbalance of the initial training data in HE-GHI-DS, deep learning models only learn the characteristics of one category, leading to low classification accuracy and weak generalization ability of models. In the GHIC task, GasHis-Transformer equally uses 140 abnormal images and 140 normal images, where the abnormal and normal images in the dataset are randomly partitioned into training, validation and test sets

Algorithm 1 GasHis-Transformer Framework

Input: The images used for training, X_{train} ; The images used for validation, X_{val} ; The images used for testing, X_{test} ; The training epoch N ;

Output: The classification presentation of the testing images y_{test} of X_{test}

- 1: Image normalization $\tilde{X}_{\text{train}} = \frac{X_{\text{train}} - \bar{X}_{\text{train}}}{\sigma}$;
 - 2: **for** current training steps n in N **do**
 - 3: Divide \tilde{X}_{train} into patches and put them into model;
 - 4: Extract global information $z_g = \text{GIM}(\tilde{X}_{\text{train}})$;
 - 5: Extract local information $z_l = \text{LIM}(\tilde{X}_{\text{train}})$;
 - 6: connect global and local information as extracted feature of model $z = [z_g, z_l]$;
 - 7: Random abandonment of neurons $\bar{z} = \text{Dropout}(z)$;
 - 8: Classification result through the full connection layer and softmax layer classification $y_{\text{train}} = \text{Softmax}(\text{FC}(\bar{z}))$;
 - 9: Model parameters $\{W_1, \dots, W_n\}$ are obtained by back propagation of the error by the optimizer;
 - 10: Put X_{val} into parameters of model $\{W_1, \dots, W_n\}$ and get classification result accuracy acc ;
 - 11: **if** The classification accuracy acc is the highest **then**
 - 12: Store the parameters of model $\{W_1, \dots, W_n\}$;
 - 13: **for** image x in X_{test} **do**
 - 14: Put x into parameters of model $\{W_1, \dots, W_n\}$ and get classification result y_{test} ;
- return** y_{test} of X_{test}

with a ratio of 1: 1: 2. Furthermore, all images are flipped horizontally and vertically and rotated 90, 180, 270 degrees to augment the training, validation and test datasets to six times. In addition, because the size of images in HE-GHI-DS is too

big to process, all of them are resized into 224×224 pixels by bilinear interpolation Smith (1981). The data setting and augmentation are shown in Table 1.

Table 1: Data setting and augmentation of gastric histopathological data for training, validation and test sets.

Image Type		Train	Validation	Test	Sum
Normal	Oringin	35	35	70	140
	Augmented	210	210	420	840
Abnormal	Oringin	35	35	70	140
	Augmented	210	210	420	840

4.1.3. Hyper-parameter Setting

GasHis-transformer is used to train the gastric histopathological image dataset for 75 epochs. AdamW optimizer Loshchilov and Hutter (2018) is used for optimization and its parameters are set as: $2e-3$ learning rate, $1e-8$ eps, $[0.9, 0.999]$ betas and $1e-2$ weight decay. AdamW solves the problem of parameter over-fitting with Adam optimizer by introducing L2 regularization terms of parameters in the loss function. It is the fastest optimizer for gradient descent speed and training neural networks which are used in all models. A learning rate adjustment strategy is used, that is, if the set loss function is not decreased within 15 epochs, the learning rate is reduced by ten times.

4.1.4. Evaluation Criteria

To evaluate the GasHis-Transformer model, the experimental result is measured by precision, recall, F1-score, accuracy and confuse matrix. True positive (TP), true negative (TN), false positive (FP) and false negative (FN) are used in the definition of these four criteria in Table 2. Precision (Pre) is a ratio of the amount of relevant information retrieved to the total amount

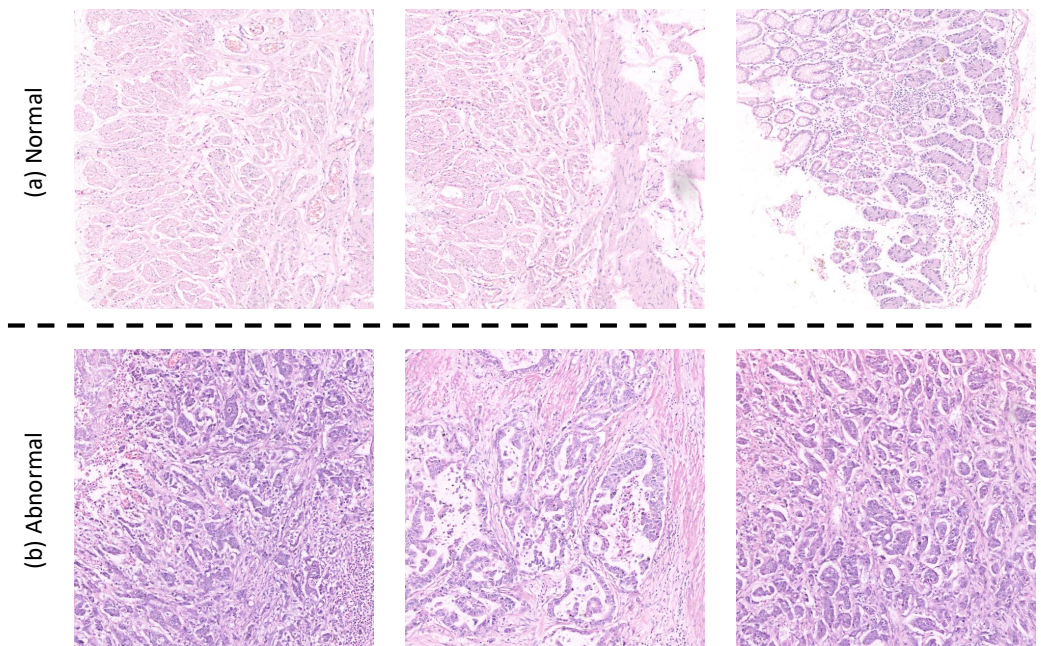


Fig. 8: Some examples in the HE-GHI-DS.

of information retrieved, which indicates how many of the predicted positive samples are real positive samples. Recall (Rec) is a ratio of the total amount of relevant information in the retrieved information system, which indicates how many positive samples in the sample have been correctly predicted. F1-score (F1) is a comprehensive consideration of precision and recall, and it is a critical evaluation criteria to evaluate a model. Accuracy (Acc) is the most typical and fundamental evaluation criteria.

Table 2: Four criteria and corresponding definitions for image classification evaluation.

Criterion	Definition	Criterion	Definition
Precision	$\frac{TP}{TP+FP}$	Recall	$\frac{TP}{TP+FN}$
F1-score	$\frac{2 \times TP}{2 \times TP + FP + FN}$	Accuracy	$\frac{TP+TN}{TP+TN+FP+FN}$

4.2. Classification Evaluation of GasHis-Transformer

4.2.1. Experimental Result

Four criteria of the validation set and the test set are calculated respectively to determine whether the GasHis-Transformer has convergence and generalization ability. The experimental results show that using GasHis-Transformer model to classify images has incomparable performance. The confusion matrix using GasHis-Transformer on the validation set and test set is shown in Fig. 9. On the validation set, 206 abnormal images and 209 normal images are classified into the correct categories. Only 4 abnormal images are misclassified as normal and 1 normal image is misclassified as abnormal. Overall, the Pre, Rec, F1 and Acc of the classification in the validation set is 99.5%, 98.1%, 98.8% and 98.8%, respectively. On the test set, 403 abnormal images and 420 normal images are classified into the correct categories. Only 17 abnormal images are misclassified as normal and even no normal images are misclassified. The Pre, Rec, F1 and Acc of the classification is 100.0%, 96.0%, 98.0% and 98.0%, respectively. Four criteria have high scores on the validation set and test set, and the differences of four criteria between validation set and test set is narrow, which proves that GasHis-Transformer has excellent generalization ability. Additionally, there are significant discrepancies among the misclassification problems that remain to be overcome, and in order to analyze the reasons of misclassification, some examples are shown in Fig. 10. In conjunction with medical knowledge from our collaborating histopathologists, the reasons for image misclassification are as follows: First, because of the complex components of histopathological images of gastric cancer, in which the features between normal and abnormal regions are inconspicuous, it leads to difficulties in image visual information description. As the example in Fig. 10 (a), it is actually intestinal metaplasia. First, due to its visual phenotype including increased cell volume and enlarged glandular structure is closed to the abnormal case, GasHis-Transformer predicts it as an incorrect result. In addition, since intestinal metaplasia is a high-risk factor for gastric cancer and is a precancerous lesion, the model highly suggests the possibility of gastric cancer. Second, some abnormal images have

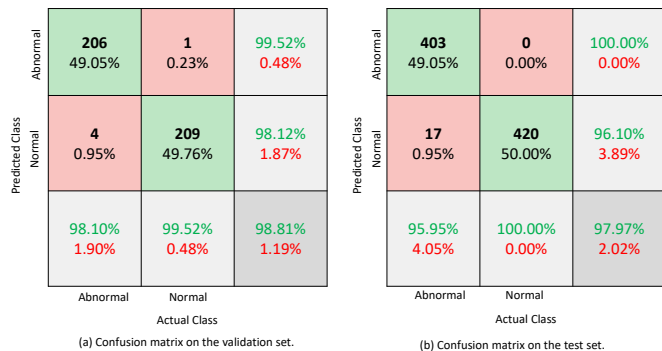


Fig. 9: Confusion matrix using GasHis-Transformer. The first column to the second column represents the confusion matrices for the classification results on the validation set, on the testing set.

the majority of regions as normal regions and just a few as abnormal regions, and the attention mechanism primarily used in the proposed GasHis-Transformer is not effective in describing all spatial in this cases. As the example in Fig. 10 (b), the abnormal tissue in the red circle only covers very limited area in the whole image (10%), which is ignored by the algorithm.

4.2.2. Contrast Experiment of GHIC

Comparison with Other Models: In order to show the performance of GasHis-Transformer in GHIC task, a contrast experiment to measure four criteria on the testing set is carried out, which compares classification performance with five CNN models and seven attention mechanism models. CNN models include VGG-16, VGG-19 Simonyan and Zisserman (2014), Inception-V3 Szegedy et al. (2016), ResNet-50 He et al. (2016), Xception Chollet (2017); attention mechanism models include Non-local+Resnet Wang et al. (2018), CBAM+Resnet Woo et al. (2018), SENet+CNN Hu et al. (2018), GCNet+Resnet Cao et al. (2019), HCRF-AM Li et al. (2021), ViT Dosovitskiy et al. (2020) and BoTNet-50 Srinivas et al. (2021). In addition, since VGG models do not converge at the learning rate of $2e-3$ using AdamW optimizer, an extra contrast experiment with a low learning rate is conducted. Finally, to prove that the image normalization leads to an excellent result in the whole process, GasHis-Transformer, classical CNN models and VT models are compared using image normalization and without image normalization.

The experimental settings of these classical CNN models and VT models are briefly conducted as follows: First, all hyper-parameters are set as the same values in Section 4.1.3. The gastric histopathological image classification result of all models is shown in Table 3. It is obvious that GasHis-Transformer achieves good performance in terms of Pre, F1 and Acc. GasHis-Transformer has some improvement compared to Xception which is the best performing of the six traditional CNN models. The two models are equal in Pre, but the proposed GasHis-Transformer has a higher Rec, F1 and Acc than Xception. In addition, the scale of our HE-GHI-DS is very limited, the pure attention mechanism method loses effectiveness in the GHIC task. Finally, although the Rec of GasHis-Transformer is not as higher as that of VGG-19, that results

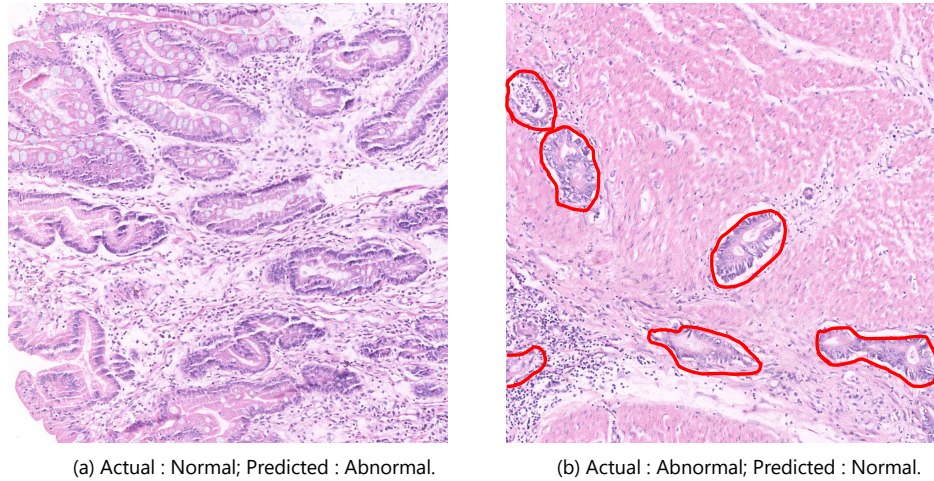


Fig. 10: Typical examples of the misclassification results.

Table 3: A comparison of GHIC using different models on HE-GHI-DS test set. ([In %].)

Model	Pre	Rec	F1	Acc
GasHis-Transformer	100.0	96.0	98.0	98.0
Xception Chollet (2017)	100.0	94.3	97.1	97.1
ResNet-50 He et al. (2016)	96.8	95.0	96.0	95.9
Inception-V3 Szegedy et al. (2016)	98.4	88.3	93.5	93.1
VGG-16 Simonyan and Zisserman (2014)	0.0	0.0	33.4	50.0
VGG-19 Simonyan and Zisserman (2014)	51.5	100.0	33.4	52.9
BotNet-50 Srinivas et al. (2021)	97.8	94.0	96.0	95.9
ViT Dosovitskiy et al. (2020)	85.8	71.9	80.0	78.2
HCRF-AM Li et al. (2021)	88.3	75.7	81.5	91.4
GCNet+Resnet Cao et al. (2019)	49.4	55.7	52.3	74.1
SENet+CNN Hu et al. (2018)	50.8	42.9	46.5	75.4
CBAM+Resnet Woo et al. (2018)	27.1	84.3	41.0	39.3
Non-local+Resnet Wang et al. (2018)	46.0	57.1	51.0	72.5

from the non-convergence of the network at a learning rate of $2e-3$. F1 of VGG-19 only achieves 33.3%, indicating that it classifies all the data in the test set as abnormal, and consequently it can be concluded that the network does not converge. The same problem also arises for VGG-16. To this end, a further experiment is carried out to optimize VGG models in next paragraph.

Comparison with Optimized VGG Models: The comparison of learning rates between $2e-3$ and $2e-4$ in VGG models is shown in Table 4, where VGG models converge at a learning rate of $2e-4$. Compared to the optimized VGG models at $2e-4$ learning rate, GasHis-Transformer has the highest Rec as well as other criteria including Pre, F1 and Acc.

Table 4: Comparison of learning rate (LR) between $2e-3$ and $2e-4$ using VGG-16 and VGG-19 Simonyan and Zisserman (2014). ([In %].)

Model	LR	Pre	Rec	F1	Acc
GasHis-Transformer	$2e-3$	100.0	96.0	98.0	98.0
VGG-16	$2e-4$	89.1	87.9	88.5	88.5
VGG-16	$2e-3$	0.0	0.0	33.4	50.0
VGG-19	$2e-4$	85.5	91.2	88.3	87.8
VGG-19	$2e-3$	51.5	100.0	33.4	52.9

Comparison with Raw Data (Without Normalization): Finally, the comparison results of pre-processing whether using normalization is shown in Fig. 11. The comparison is performed with VGG-16 and VGG-19 using a learning rate of $2e-4$ together with other networks using the original setting. There is a clear trend of increasing these four criteria when using normalization. For the Pre, the results obtained using normalization have a significant improvement for most models. Especially, ViT even has a significant improvement of 23.4%. Other models including GasHis-Transformer, BotNet-50, Inception-V3, VGG-16 and VGG-19 improve by 5.1%, 5%, 5.5%, 5.5% and 6.5%, respectively. The criteria of Xception remain constant after using normalization, and only the criteria of ResNet-50 becomes worse after using normalization. For Rec, while Inception-V3, VGG-16, VGG-19 and ViT have different degrees of reduction after using normalization, models with high classification outcomes including GasHis-Transformer, Xception, BotNet-50 and ResNet-50 all have an improvement around 3%. For F1 and Acc, which are the overall criteria for evaluating a model's performance, all models show some improvement after using normalization. In summary, the

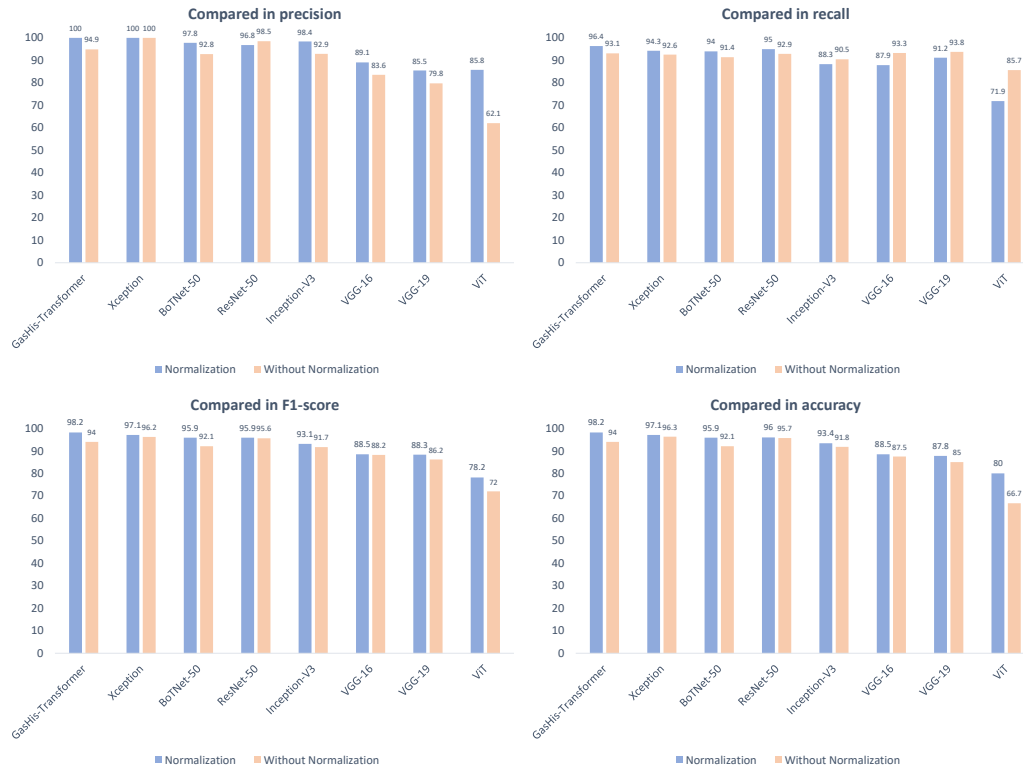


Fig. 11: Comparison of pre-inception processing whether using normalization between GasHis-Transformer and other models.

use of normalization in image preprocessing can promote four criteria of most models.

4.2.3. Robustness Test of GasHis-Transformer

Robustness is a property that maintains systems' stability under parameter ingestion and measures behaviour of systems under non-standard conditions. Robustness is defined by community as the degree to which a system operates correctly in the presence of exceptional inputs or stressful environmental conditions Micskei et al. (2012). The goal of robustness test is that the models work correctly with each functional module when handling incorrect data and abnormal problems (through adding noise or taking other datasets), enhancing models' fault resistance. To test the robustness of the proposed GasHis-Transformer model, ten different adversarial attacks and conventional noises are added to the HE-GHI-DS test set. Adversarial attacks include FGM Goodfellow et al. (2014), FSGM Kurakin et al. (2016), PGD Madry et al. (2017) and Deepfool Moosavi-Dezfooli et al. (2016); conventional noises include Gaussian noise, Salt & Pepper noise, uniform noise, exponential noise, Rayleigh noise and Erlang noise Verma and Ali (2013). First, the epsilons are performed with nine levels in $[0.001, 0.256]$ using 0.001 as initialization and the powers of 2 as step length. Then, Pre, Rec, F1 and Acc are used to evaluate the robustness of GasHis-Transformer in the GHIC task. Fig. 12 shows four criteria under different epsilons and noise.

For adversarial attacks noises, first, GasHis-Transformer is optimally robust when FGM is increased, and different epsilons have almost no effect on the model. Secondly, although criteria obtained by adding FSGM have some differences com-

pared with adding FGM, in general, the performance is positive. When epsilon is higher than 0.032, the criteria converge to stability, even Rec increases slightly. Finally, adding Deepfool and PGD of any magnitude of epsilons results in a poor classification of the model. In summary, for noise generation by adversarial attacks, GasHis-Transformer has better robustness to FGM and FSGM.

For conventional noises, first, while four criteria of adding Erlang noise and uniform noise decrease compared to those of FGM in adversarial attacks, they are relatively constant compared to those with other convention noises. Therefore, adding them does not affect the robustness of the model in general. In addition, when epsilon is lower than 0.1, the model is barely affected by adding Gaussian noise, Rayleigh noise and Salt & Pepper noise. But when epsilon is higher than 0.1, the Pre, Rec and F1 of the test set drop to 0, which indicates that all images in the abnormal category are misclassified as normal. In summary, for convention noises, GasHis-Transformer has strong robustness to both Erlang noise and uniform noise. Similarly, the model also has strong robustness of epsilon between 0 and 0.1 for Gaussian noise, Rayleigh noise and Salt & Pepper noise.

4.3. Extended Experiment

In this section, firstly, an extended experiment for gastrointestinal cancer identification is done using extra 620 gastrointestinal images. Then, extended experiments are performed on a publicly available lymphoma dataset immunohistochemical (IHC) stained lymphoma histopathological image dataset (IHC-LI-DS) Jaffe and Orlov (2008) and a breast cancer dataset BreakHis Spanhol et al. (2015). The experimental setup of the

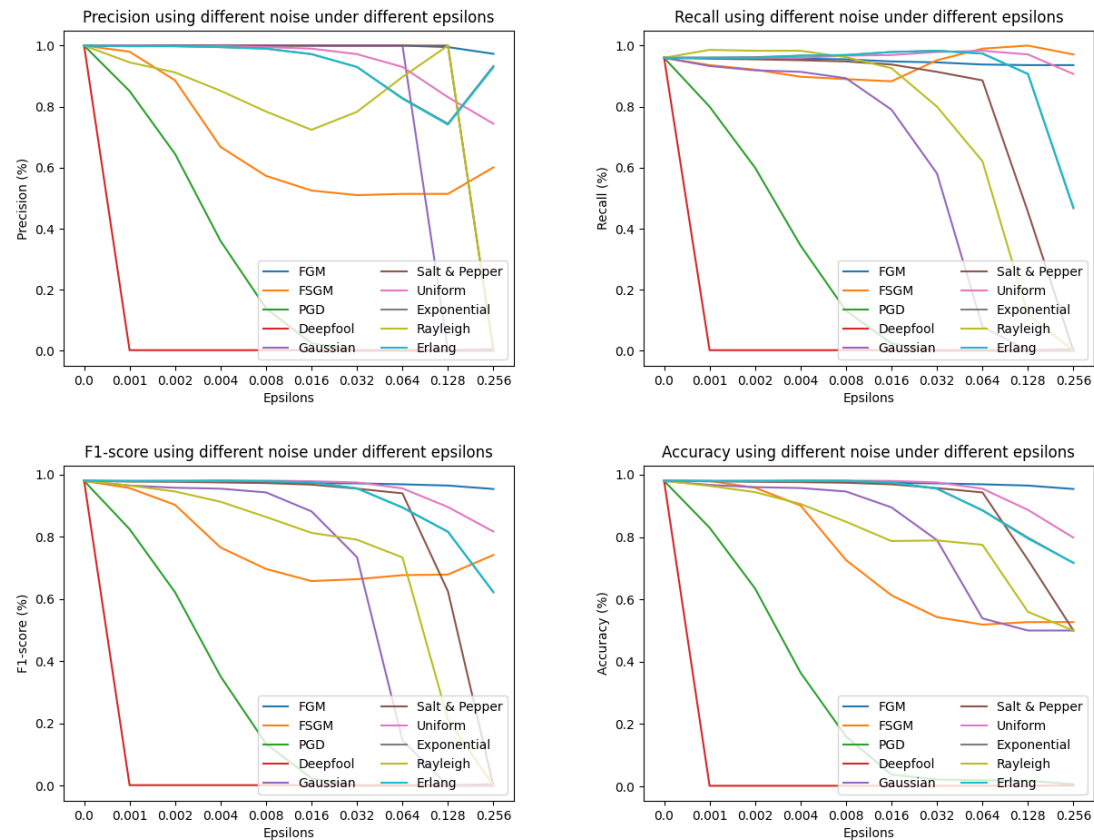


Fig. 12: Robustness test of GasHis-Transformer under ten adversarial attack and conventional noises.

extended experiments is generally based on the gastric cancer dataset and slightly adjusted with their respective characteristics.

4.3.1. Extended Experiment for Gastrointestinal Cancer Identification

Gastrointestinal cancer includes gastric cancer and intestinal cancer. They are both digestive system cancer. Due to gastric and intestinal organs have glands, their histopathological images have many similar features Inoue *et al.* (2020). An example of gastrointestinal cancer histopathological images is shown in Fig. 13. This extended experiment is used to evident that not only GasHis-Transformer model has outstanding performance in GHIC task, in addition to the same way, but also it has an excellent performance in the gastrointestinal cancer identification task. Based on the main experiment in Sec. 4.2.1, medical doctors are often focus more on the identification of abnormal category. If an image identifies as abnormal by deep learning models, doctors need to conduct operations such as staging benign and malignant lesions, determining the area of the lesion, and determining whether it has spread extensively. Therefore, in clinical applications, doctors frequently prefer models with high identification rates in abnormal category. In the gastrointestinal cancer identification task, 620 gastrointestinal cancer images including 420 gastric cancer images and 200 intestinal cancer images are used to test GasHis-Transformer. The

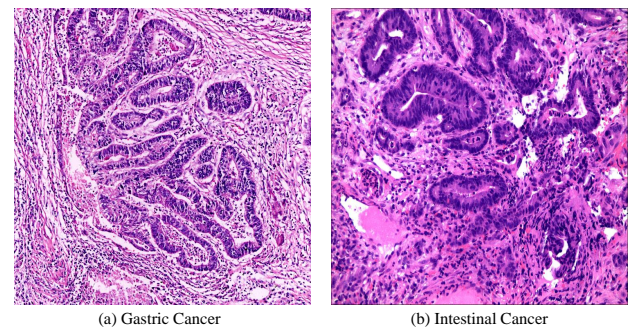


Fig. 13: An example of gastrointestinal cancer.

gastrointestinal cancer identification results are as follow: For gastric cancer images, 404 gastric cancer images are precisely identified by the model, and only 16 gastric cancer images are not identified, where Acc of the model for gastric cancer images reaches 96.2%; for intestinal cancer images, 196 intestinal cancer images are identified by the model, only 4 intestinal cancer images are not identified. Acc of the model for intestinal images reaches 98.0%. In summary, 620 gastrointestinal images including 600 identified images and 20 unidentified images obtain an identification Acc of 96.8%.

4.3.2. Extended Experiment for Breast Cancer Image Classification

Breast cancer is considered the most common type of cancer amongst women. Breast cancer is associated with a high mortality rate in comparison with other cancers Waks and Winer (2019). We further demonstrate the well-performance of GasHis-Transformer in breast cancer image classification using BreakHis dataset Spanhol et al. (2015). BreakHis consists of 7909 images at various magnifications including 40 \times , 100 \times , 200 \times and 400 \times , using H&E stained, categorized into benign and malignant tumors. The size of images is 700 \times 460 pixels and with ".png" format. Both benign and malignant breast tumors can be classified into four different sub-types. In this paper, malignant tumors with a magnification of 200 \times are used for the four classifications including ductal carcinoma (DC), lobular carcinoma (LC), mucinous carcinoma (MC) and papillary carcinoma (PC) of the breast. An example of 200 \times BreakHis images is shown in Fig. 14 and the original data setting and augmentation are shown in Table 5. The original data is partitioned with a ratio of 6: 2: 2 for training, validation and test sets.

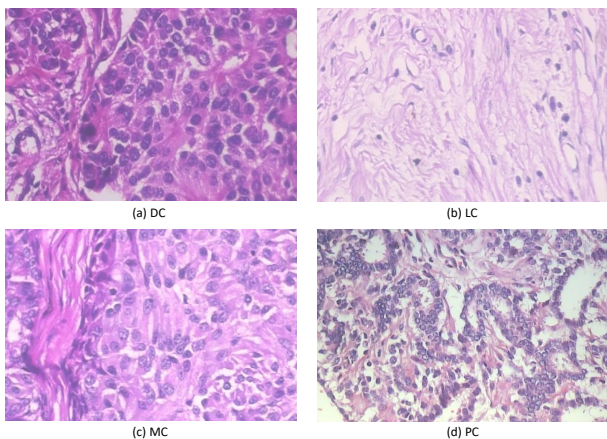


Fig. 14: An example of 200 \times BreakHis Images.

Table 5: Data setting and augmentation of BreakHis dataset for training, validation and test sets.

Image Type		Train	Validation	Test	Sum
DC	Oringin	538	179	179	896
	Augmented	3228	1074	1074	5376
LC	Oringin	98	33	32	163
	Augmented	588	198	192	978
MC	Oringin	118	39	39	196
	Augmented	708	234	234	1176
PC	Oringin	81	27	27	135
	Augmented	486	162	162	810

The same experimental parameter setting is used for the classification of BreakHis data as that for HE-GHI-DS. The best classification result of traditional CNN models on BreakHis dataset is Inception-V3, where four criteria including Pre, Rec, F1 and Acc are 88.0%, 84.6%, 84.2% and 88.0%, respectively.

Table 6: A comparison of breast cancer image classification results using different models on BreakHis test set. ([In %].)

Model	Pre	Rec	F1	Acc
GasHis-Transformer	85.3	86.1	85.6	89.4
Xception Chollet (2017)	80.1	80.3	80.2	86.0
ResNet-50 He et al. (2016)	71.7	74.7	72.7	81.3
Inception-V3 Szegedy et al. (2016)	88.0	84.6	84.2	88.0
VGG-16 Simonyan and Zisserman (2014)	80.9	76.2	77.7	84.5
VGG-19 Simonyan and Zisserman (2014)	79.8	80.6	80.1	85.6
BotNet-50 Srinivas et al. (2021)	77.0	74.2	74.8	83.6
ViT Dosovitskiy et al. (2020)	70.9	77.5	73.6	80.1

Compared with Inception-V3, although the Pre of GasHis-Transformer decreases marginally, its Rec, F1 and Acc are increased by 1.5%, 1.4% and 1.4%, respectively. While a high precision can only demonstrate the conservativeness of the models and only forecast highly sure samples, F1 and Acc are the comprehensive indicator for determining a model, so it shows that GasHis-Transformer has better image classification performance on the BreakHis dataset. A comparison of extended experiment using different models on BreakHis test set is shown in Table 6.

The expansion experiment on the BreakHis dataset illustrates that GasHis-Transformer, which uses GIM and LIM, integrated the advantages of CNN and Transformer models and can classify breast cancer well. Its classification performance exceeds those of the current predominant CNN and VT models. The experiment result further demonstrates that GasHis-Transformer is not only outstanding in GHIC tasks, but also capable in other cancer histopathological image using H&E strained classification tasks.

4.3.3. Extended Experiment for Lymphoma Image Classification

Malignant lymphoma is a cancer that affects the lymph nodes. Three types of malignant lymphoma are representative in the dataset: chronic lymphocytic leukemia (CLL), follicular lymphoma (FL) and mantle cell lymphoma (MCL) Lennert et al. (1975). An example of the immunohistochemical (IHC) stained lymphoma histopathological image dataset (IHC-LI-DS) is shown in Fig. 15. The data setting and augmentation of lymphoma cancer datasets for training, validation and test sets is shown in Table 7. A total of 374 images of different cancer categories are available in the IHC-LI-DS. The number of CLL images is 113, the number of FL images is 139 and the number of MCL images is 122. All images in the lymphoma dataset are 1388 \times 1040 pixels in size with ".tif" format. Since three different types of lymphoma are classified according to the shape of

lymphocytes, directly resizing the image of lymphoma makes it difficult to distinguish the small and dense lymphocytes. Therefore, we crop the whole lymphoma image into 224×224 pixels as the standard input of GasHis-Transformer to argument the datasets by 24 times.

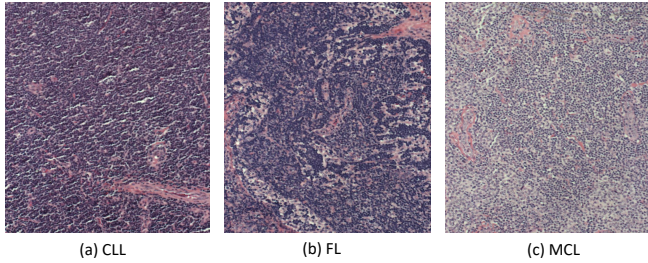


Fig. 15: An example of IHC-LI-DS Images.

Table 7: Data setting and augmentation of IHC-LI-DS for training, validation and test sets.

Image Type		Train	Validation	Test	Sum
CLL	Oringin	40	30	43	113
	Augmented	960	720	1032	2712
FL	Oringin	40	30	69	139
	Augmented	960	720	1656	3336
MCL	Oringin	40	30	52	122
	Augmented	960	720	1248	2928

Table 8 illustrates four criteria using GasHis-Transformer, Inception-V3 Szegedy et al. (2016), ResNet-50 He et al. (2016), Xception Chollet (2017), ViT Dosovitskiy et al. (2020), and BoTNet-50 Srinivas et al. (2021) at learning rate as $2e-3$ and VGG-16 and VGG-19 Simonyan and Zisserman (2014) at the learning rate as $2e-4$ to classify three-class lymphoma dataset which like something has been done in gastric dataset. GasHis-Transformer has the best performance in all four criteria compared with other traditional models. In the IHC-LI-DS, the best performance of the traditional models is Inception-V3, Inception-V3 has the highest Pre, Rec, F1 and Acc in traditional CNN models, which are 79.0%, 78.7%, 78.7% and 80.2%, respectively. However, the performance of GasHis-Transformer is even better than that of Inception-V3. Pre, Rec, F1 and Acc of GasHis-Transformer reach an outstanding 82.6%, 83.0%, 82.8% and 83.9%, respectively. Compared with Inception-V3, they have improved by 2.9%, 3.0%, 2.9% and 2.0%, respectively. Therefore, on IHC-LI-DS, like on HE-GHI-DS and BreakHis dataset, GasHis-Transformer exhibits favorable classification skills.

The expanded experiment on the IHC-LI-DS demonstrates that GasHis-Transformer not only has an excellent performance in datasets stained by H&E stained but also the favorable classification skills in IHC stained datasets.

4.4. Experimental Environment and Computational Time

Finally, the computation time of GasHis-Transformer model is briefly depicted. A workstation with Windows 10, AMD

Table 8: A comparison of lymphoma cancer image classification results using different models on IHC-LI-DS test set. ([In %].)

Model	Pre	Rec	F1	Acc
GasHis-Transformer	82.6	83.0	82.8	83.9
Xception Chollet (2017)	79.7	79.4	78.4	80.1
ResNet-50 He et al. (2016)	78.7	79.3	78.6	79.7
Inception-V3 Szegedy et al. (2016)	79.7	80.0	79.9	80.9
VGG-16 Simonyan and Zisserman (2014)	75.3	75.7	75.4	76.9
VGG-19 Simonyan and Zisserman (2014)	76.8	77.3	76.8	77.8
BotNet-50 Srinivas et al. (2021)	79.0	78.7	78.7	80.2
ViT Dosovitskiy et al. (2020)	71.4	72.3	71.2	72.6

Ryzen 7 4800HS with Radeon Graphics with 2.90 GHz, GeForce RTX 2060 with 6 GB and 16 GB RAM is utilized in the experiment. The Matlab of R2020b is utilized to do the pre-processing of original images. When training GasHis-Transformer, Xception, BoTNet-50, ResNet-50, Inception-V3, VGG-16, VGG-19 and ViT, PyTorch v1.6 framework of Python 3.6 is deployed. Table 9 shows the parameter size (PS) and training time on datasets of three different cancers including gastric (G), breast (B) and lymphoma (L) of all eight models including GasHis-Transformer, Xception, BoTNet-50, ResNet-50, Inception-V3, VGG-16, VGG-19 and ViT.

Table 9: The PS (MB) and training time (hour) of all eight models.

Models	PS	Training Time		
		G	B	L
GasHis-Transformer	155	0.86	2.78	2.39
Xception Chollet (2017)	79	0.75	2.36	1.75
ResNet-50 He et al. (2016)	90	0.69	1.73	1.46
Inception-V3 Szegedy et al. (2016)	83	0.73	1.58	1.58
VGG-16 Simonyan and Zisserman (2014)	268	0.78	2.39	1.78
VGG-19 Simonyan and Zisserman (2014)	298	0.81	2.76	2.01
BotNet-50 Srinivas et al. (2021)	72	0.69	1.72	1.46
ViT Dosovitskiy et al. (2020)	48	0.69	1.58	1.29

5. Conclusion and Future Work

In this paper, we propose a GasHis-Transformer to classify histopathological images of gastric cancer into normal or abnor-

mal in a binary classification. This approach not only considers the advantages of classical CNN model in describing local information but also uses the most recent Transformer model for global information description. GasHis-Transformer considers the global and local associations of images in a spatial context. In the experiment, the method is tested on a gastric cancer histopathological dataset with an accuracy of 98.0% for classification, which demonstrates its potential in GHIC tasks. In addition, we conduct a gastrointestinal cancer identification task to demonstrate that GasHis-Transformer model has an excellent cancer identification ability. Finally, we carry out extended tests on the breast cancer dataset and the lymphoma dataset with accuracies of 89.4% and 83.9%, respectively, demonstrating the generalization capability both in H&E stained and IHC stained of GasHis-Transformer on histopathological images.

In our future work, we plan to increase the volume of data in a single dataset, allowing the same doctors to expand the data. This will generalize testing the model not only on gastric cancer but also on more cancer types, such as liver or intestinal cancer. In addition, we will try to improve the Transformer model by developing new network structures.

Acknowledgements

This work is supported by National Natural Science Foundation of China (No. 61806047). We thank Miss Zixian Li and Mr. Guoxian Li for their important discussion.

Conflict of Interest

The authors declare that they have no conflict of interest.

Author Contributions

Haoyuan Chen: Method, experiment, result analysis and paper writing;

Chen Li: Corresponding author, method, research organization, data organization, result analysis, paper writing, proofreading and funding support;

Ge Wang: Corresponding author, method, result analysis, paper writing and proofreading;

Xiaoyan Li: Data, medical knowledge support and result analysis;

Weiming Hu: Data and experiment;

Yixin Li: Experiment and proofreading;

Wanli Liu: Experiment;

Changhao Sun: Method;

Marcin Grzegorzec: Research organization and funding support.

References

Asiri, N., Hussain, M., Al Adel, F., Alzaidi, N., 2019. Deep learning based computer-aided diagnosis systems for diabetic retinopathy: A survey. *Artificial intelligence in medicine* 99, 101701.

Baldi, P., Sadowski, P.J., 2013. Understanding dropout. *Advances in neural information processing systems* 26, 2814–2822.

Bello, I., Zoph, B., Vaswani, A., Shlens, J., Le, Q.V., 2019. Attention augmented convolutional networks, in: *Proceedings of the IEEE/CVF International Conference on Computer Vision*, pp. 3286–3295.

Burkhardt, R., 2012. *Bone marrow and bone tissue: color atlas of clinical histopathology*. Springer Science & Business Media.

Cao, Y., Xu, J., Lin, S., Wei, F., Hu, H., 2019. Gcnet: Non-local networks meet squeeze-excitation networks and beyond, in: *Proceedings of the IEEE/CVF International Conference on Computer Vision Workshops*, pp. 0–0.

Chan, A.O.O., Wong, B.C.Y., Lam, S.K., 2001. Gastric cancer: past, present and future. *Canadian Journal of Gastroenterology* 15, 469–474.

Cho, K.O., Lee, S.H., Jang, H.J., 2020. Feasibility of fully automated classification of whole slide images based on deep learning. *The Korean journal of physiology & pharmacology: official journal of the Korean Physiological Society and the Korean Society of Pharmacology* 24, 89.

Chollet, F., 2017. Xception: Deep learning with depthwise separable convolutions, in: *Proceedings of the IEEE conference on computer vision and pattern recognition*, pp. 1251–1258.

Doi, K., 2005. Current status and future potential of computer-aided diagnosis in medical imaging. *The British journal of radiology* 78, s3–s19.

Doi, K., 2007. Computer-aided diagnosis in medical imaging: historical review, current status and future potential. *Computerized medical imaging and graphics* 31, 198–211.

Dosovitskiy, A., Beyer, L., Kolesnikov, A., Weissenborn, D., Zhai, X., Unterthiner, T., Dehghani, M., Minderer, M., Heigold, G., Gelly, S., et al., 2020. An image is worth 16x16 words: Transformers for image recognition at scale. *arXiv preprint arXiv:2010.11929*.

Elsheikh, T.M., Austin, R.M., Chhieng, D.F., Miller, F.S., Moriarty, A.T., Renshaw, A.A., 2013. American society of cytopathology workload recommendations for automated pap test screening: Developed by the productivity and quality assurance in the era of automated screening task force. *Diagnostic cytopathology* 41, 174–178.

Finlayson, G.D., Schiele, B., Crowley, J.L., 1998. Comprehensive colour image normalization, in: *European conference on computer vision*, Springer. pp. 475–490.

García, E., Hermoza, R., Castanon, C.B., Cano, L., Castillo, M., Castaneda, C., 2017. Automatic lymphocyte detection on gastric cancer ihc images using deep learning, in: *2017 IEEE 30th international symposium on computer-based medical systems (CBMS)*, IEEE. pp. 200–204.

Goodfellow, I.J., Shlens, J., Szegedy, C., 2014. Explaining and harnessing adversarial examples. *arXiv preprint arXiv:1412.6572*.

Han, K., Wang, Y., Chen, H., Chen, X., Guo, J., Liu, Z., Tang, Y., Xiao, A., Xu, C., Xu, Y., et al., 2020. A survey on visual transformer. *arXiv preprint arXiv:2012.12556*.

He, K., Zhang, X., Ren, S., Sun, J., 2016. Deep residual learning for image recognition, in: *Proceedings of the IEEE conference on computer vision and pattern recognition*, pp. 770–778.

Howard, A.G., Zhu, M., Chen, B., Kalenichenko, D., Wang, W., Weyand, T., Andreetto, M., Adam, H., 2017. Mobilenets: Efficient convolutional neural networks for mobile vision applications. *arXiv preprint arXiv:1704.04861*.

Hu, J., Shen, L., Sun, G., 2018. Squeeze-and-excitation networks, in: *Proceedings of the IEEE conference on computer vision and pattern recognition*, pp. 7132–7141.

Huang, J., Qu, L., Jia, R., Zhao, B., 2019. O2u-net: A simple noisy label detection approach for deep neural networks, in: *Proceedings of the IEEE/CVF International Conference on Computer Vision*, pp. 3326–3334.

Inoue, A., Ota, S., Nitta, N., Murata, K., Shimizu, T., Sonoda, H., Tani, M., Ban, H., Inatomi, O., Ando, A., et al., 2020. Difference of computed tomographic characteristic findings between gastric and intestinal gastrointestinal stromal tumors. *Japanese journal of radiology* 38, 771–781.

Jaffe, E., Orlov, N., 2008. Nia intramural research program laboratory of genetics. <https://ome.grc.nia.nih.gov/iicbu2008/lymphoma/index.html>.

Khan, S., Naseer, M., Hayat, M., Zamir, S.W., Khan, F.S., Shah, M., 2021. Transformers in vision: A survey. *arXiv preprint arXiv:2101.01169*.

Korkmaz, S.A., Binol, H., 2018. Classification of molecular structure images by using ann, rf, lbp, hog, and size reduction methods for early stomach cancer detection. *Journal of Molecular Structure* 1156, 255–263.

Korkmaz, S.A., Bınoł, H., Akçıçek, A., Korkmaz, M.F., 2017. A expert system for stomach cancer images with artificial neural network by using hog features and linear discriminant analysis: Hog_lda.ann, in: *2017 IEEE 15th International Symposium on Intelligent Systems and Informatics (SISY)*, IEEE. pp. 000327–000332.

- Kosaraju, S.C., Hao, J., Koh, H.M., Kang, M., 2020. Deep-hipo: Multi-scale receptive field deep learning for histopathological image analysis. *Methods* 179, 3–13.
- Krizhevsky, A., Sutskever, I., Hinton, G.E., 2012. Imagenet classification with deep convolutional neural networks. *Advances in neural information processing systems* 25, 1097–1105.
- Kurakin, A., Goodfellow, I., Bengio, S., et al., 2016. Adversarial examples in the physical world.
- LeCun, Y., Bengio, Y., Hinton, G., 2015. Deep learning. *nature* 521, 436–444.
- LeCun, Y., Boser, B., Denker, J.S., Henderson, D., Howard, R.E., Hubbard, W., Jackel, L.D., 1989. Backpropagation applied to handwritten zip code recognition. *Neural computation* 1, 541–551.
- Lennert, K., Mohri, N., Stein, H., Kaiserling, E., 1975. The histopathology of malignant lymphoma. *British Journal of Haematology* 31, 193–203.
- Li, Y., Li, X., Xie, X., Shen, L., 2018. Deep learning based gastric cancer identification, in: 2018 IEEE 15th International Symposium on Biomedical Imaging (ISBI 2018), IEEE. pp. 182–185.
- Li, Y., Wu, X., Li, C., Sun, C., Rahaman, M., Chen, H., Yao, Y., Li, X., Zhang, Y., Jiang, T., 2021. A hierarchical conditional random field-based attention mechanism approach for gastric histopathology image classification. *arXiv preprint arXiv:2102.10499*.
- Liu, B., Zhang, M., Guo, T., Cheng, Y., 2018. Classification of gastric slices based on deep learning and sparse representation, in: 2018 Chinese Control And Decision Conference (CCDC), IEEE. pp. 1825–1829.
- Liu, W., Wen, Y., Yu, Z., Yang, M., 2016. Large-margin softmax loss for convolutional neural networks., in: *ICML*, p. 7.
- Loshchilov, I., Hutter, F., 2018. Fixing weight decay regularization in adam.
- Lu, Z., Bai, Y., Chen, Y., Su, C., Lu, S., Zhan, T., Hong, X., Wang, S., 2020. The classification of gliomas based on a pyramid dilated convolution resnet model. *Pattern Recognition Letters* 133, 173–179.
- Madry, A., Makelov, A., Schmidt, L., Tsipras, D., Vladu, A., 2017. Towards deep learning models resistant to adversarial attacks. *arXiv preprint arXiv:1706.06083*.
- Micskei, Z., Madeira, H., Avritzer, A., Majzik, I., Vieira, M., Antunes, N., 2012. Robustness testing techniques and tools, in: *Resilience Assessment and Evaluation of Computing Systems*. Springer, pp. 323–339.
- Miettinen, M., Lasota, J., et al., 2003. Gastrointestinal stromal tumors (gists): definition, occurrence, pathology, differential diagnosis and molecular genetics. *Pol J pathol* 54, 3–24.
- Moosavi-Dezfooli, S.M., Fawzi, A., Frossard, P., 2016. Deepfool: a simple and accurate method to fool deep neural networks, in: *Proceedings of the IEEE conference on computer vision and pattern recognition*, pp. 2574–2582.
- Ramachandran, P., Parmar, N., Vaswani, A., Bello, I., Levskaya, A., Shlens, J., 2019. Stand-alone self-attention in vision models. *arXiv preprint arXiv:1906.05909*.
- Rawat, W., Wang, Z., 2017. Deep convolutional neural networks for image classification: A comprehensive review. *Neural computation* 29, 2352–2449.
- Sharma, H., Zerbe, N., Böger, C., Wienert, S., Hellwich, O., Hufnagl, P., 2017. A comparative study of cell nuclei attributed relational graphs for knowledge description and categorization in histopathological gastric cancer whole slide images, in: 2017 IEEE 30th International Symposium on Computer-Based Medical Systems (CBMS), IEEE. pp. 61–66.
- Sharma, H., Zerbe, N., Heim, D., Wienert, S., Behrens, H.M., Hellwich, O., Hufnagl, P., 2015. A multi-resolution approach for combining visual information using nuclei segmentation and classification in histopathological images., in: *VISAPP (3)*, pp. 37–46.
- Shaw, P., Uszkoreit, J., Vaswani, A., 2018. Self-attention with relative position representations. *arXiv preprint arXiv:1803.02155*.
- Sifre, L., Mallat, S., 2014. Rigid-motion scattering for texture classification. *arXiv preprint arXiv:1403.1687*.
- Simonyan, K., Zisserman, A., 2014. Very deep convolutional networks for large-scale image recognition. *arXiv preprint arXiv:1409.1556*.
- Smith, P., 1981. Bilinear interpolation of digital images. *Ultramicroscopy* 6, 201–204.
- Song, Z., Zou, S., Zhou, W., Huang, Y., Shao, L., Yuan, J., Gou, X., Jin, W., Wang, Z., Chen, X., et al., 2020. Clinically applicable histopathological diagnosis system for gastric cancer detection using deep learning. *Nature communications* 11, 1–9.
- Spanhol, F.A., Oliveira, L.S., Petitjean, C., Heutte, L., 2015. A dataset for breast cancer histopathological image classification. *Ieee transactions on biomedical engineering* 63, 1455–1462.
- Srinivas, A., Lin, T.Y., Parmar, N., Shlens, J., Abbeel, P., Vaswani, A., 2021. Bottleneck transformers for visual recognition. *arXiv preprint arXiv:2101.11605*.
- Srivastava, N., Hinton, G., Krizhevsky, A., Sutskever, I., Salakhutdinov, R., 2014. Dropout: a simple way to prevent neural networks from overfitting. *The journal of machine learning research* 15, 1929–1958.
- Sun, C., Li, C., Li, Y., 2020. Data for hcrf. <http://dx.doi.org/10.17632/thgfh23xgy7.2/>. Mendeley data, v2.
- Szegedy, C., Liu, W., Jia, Y., Sermanet, P., Reed, S., Anguelov, D., Erhan, D., Vanhoucke, V., Rabinovich, A., 2015. Going deeper with convolutions, in: *Proceedings of the IEEE conference on computer vision and pattern recognition*, pp. 1–9.
- Szegedy, C., Vanhoucke, V., Ioffe, S., Shlens, J., Wojna, Z., 2016. Rethinking the inception architecture for computer vision, in: *Proceedings of the IEEE conference on computer vision and pattern recognition*, pp. 2818–2826.
- Vaswani, A., Shazeer, N., Parmar, N., Uszkoreit, J., Jones, L., Gomez, A.N., Kaiser, L., Polosukhin, I., 2017. Attention is all you need. *arXiv preprint arXiv:1706.03762*.
- Verma, R., Ali, J., 2013. A comparative study of various types of image noise and efficient noise removal techniques. *International Journal of advanced research in computer science and software engineering* 3.
- Waks, A.G., Winer, E.P., 2019. Breast cancer treatment: a review. *Jama* 321, 288–300.
- Wang, X., Girshick, R., Gupta, A., He, K., 2018. Non-local neural networks, in: *Proceedings of the IEEE conference on computer vision and pattern recognition*, pp. 7794–7803.
- Woo, S., Park, J., Lee, J.Y., Kweon, I.S., 2018. Cbam: Convolutional block attention module, in: *Proceedings of the European conference on computer vision (ECCV)*, pp. 3–19.
- Yassin, N.I., Omran, S., El Houbay, E.M., Allam, H., 2018. Machine learning techniques for breast cancer computer aided diagnosis using different image modalities: A systematic review. *Computer methods and programs in biomedicine* 156, 25–45.
- Yis, O.M., Bugdayci, G., Pehlivan, M.B., Basol, M., 2019. Roles of the systemic inflammatory response biomarkers in the diagnosis of cancer patients with solid tumors. *Experimental Biomedical Research* 2, 37–43.